Preprint of: supporting information for Hybrid polyhedral oligomeric silsesquioxanes-imides with tailored intercage spacing for sieving of hot gases, 2014, **26**, (12), 3660-3664, http://pubs.acs.org/doi/abs/10.1021/cm500691e

Hybrid polyhedral oligomeric silsesquioxanes-imides with tailored intercage spacing for sieving of hot gases

Michiel J.T. Raaijmakers [†], Matthias Wessling [‡], Arian Nijmeijer [†] and Nieck E. Benes [*,†]

Supporting Information

Scheme S1. Formation of polyPOSS-(amic acid) and polyPOSS-imide network by interfacial polymerization. (a) Partial deprotonation of the octa-ammonium POSS by sodium hydroxide to create amine functionalized functional groups. (b) Interfacial polycondensation reaction of the partially amine-functionalized POSS cage and the different dianhydrides, resulting in the formation of polyPOSS-(amic acid)s. (c) thermal conversion

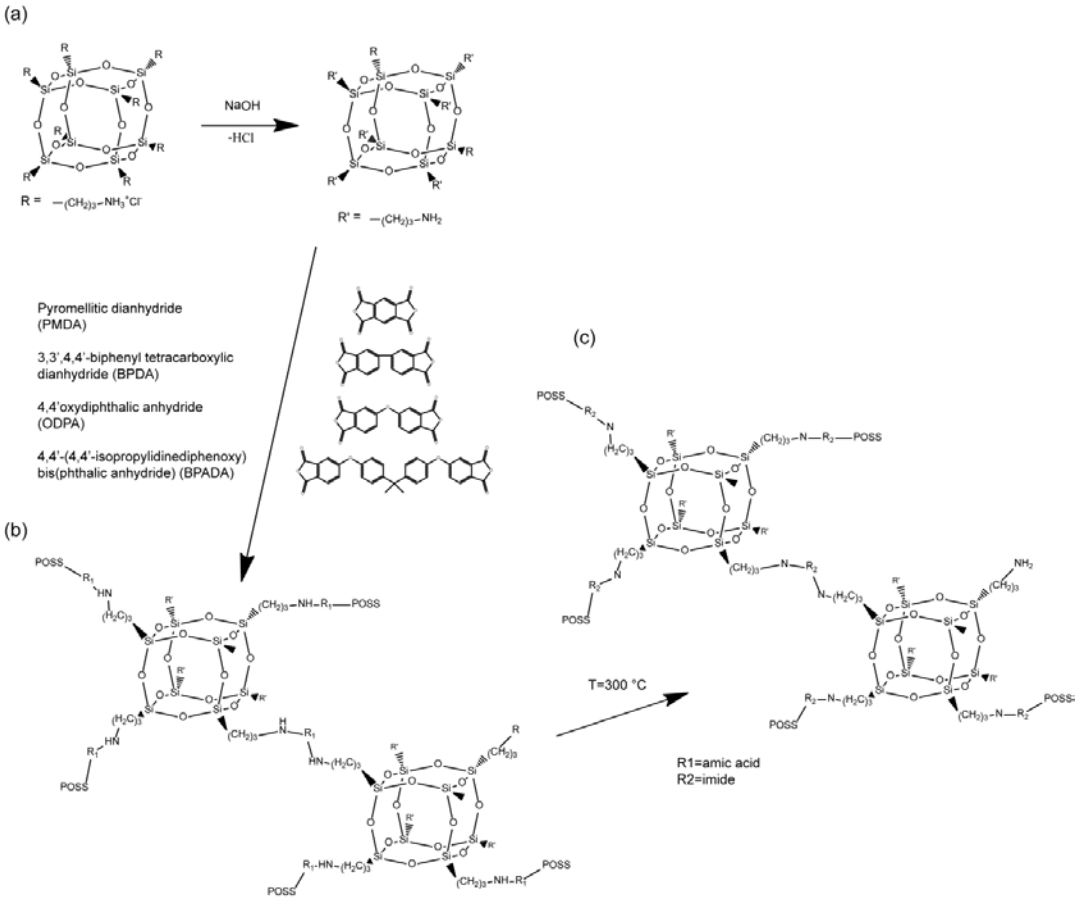

Reaction scheme S1 shows the formation of polyPOSS-(amic acid) and polyPOSS-imide network by interfacial polymerization. Ammonium chloride salt functionalized POSS is readily dissolved in water. Subsequently, the pH of the solution is adjusted using sodium hydroxide (1 M) to allow the conversion of ammonium to primary amine functional groups. The alkaline aqueous POSS solution is contacted with a dianhydride solution in toluene for 5 minutes. The polycondensation reaction at the interface results in rapid and defect-free layer formation of the hybrid polyPOSS-(amic acid) network. After removal of the reactants, by flushing with acetone, the layers are heat treated at 300 °C in an air atmosphere to convert the polyPOSS-(amic acid)s to polyPOSS-imides.

Material characterization

Gas permeation analysis. Membrane single gas permeation experiments were performed on an in-house developed gas permeation setup, using Kalrez® Spectrum 6375 O-rings. All

membranes were measured in a dead-end mode at a trans-membrane pressure of 2 bar, and atmospheric pressure at the permeate side. The membranes were heated under helium atmosphere at a heating rate of 1.5 °C/min. When the helium permeance reached a constant value, the other gases (N_2, CH_4, H_2, and CO_2, consecutively) were measured at temperatures between 50-300 °C. Equilibration time between measurements was at least 30 minutes.

Figure S1 shows the Arrhenius plots of the *log*(permeance) as function of $R^{-1}T^{-1} \cdot 10^{-3}$ for the membranes prepared with PMDA and ODPA. Both membranes show higher permeation rate with increasing temperatures. The activation energies for gas permeation through PMDA based polyPOSS-imides remain similar over the complete temperature range. The corresponding ideal gas selectivities of H_2/N_2, H_2/CH_4, H_2/CO_2 and CO_2/CH_4 as a function of temperature for the polyPOSS-imides derived from PMDA (**d**) show H_2/N_2 and H_2/CH_4 selectivities between 10-55. The low activation energy for N_2 and CH_4 substantiates that the short imide bridges do not exhibit macromolecular mobility that is required for transport of large kinetic diameter gases. This is in contrast to the apparent activation energies for N_2 and CH_4 for (c) BPADA polyPOSS-imides. The higher mobility of the large kinetic diameter gases originates from the larger imide bridge distance.

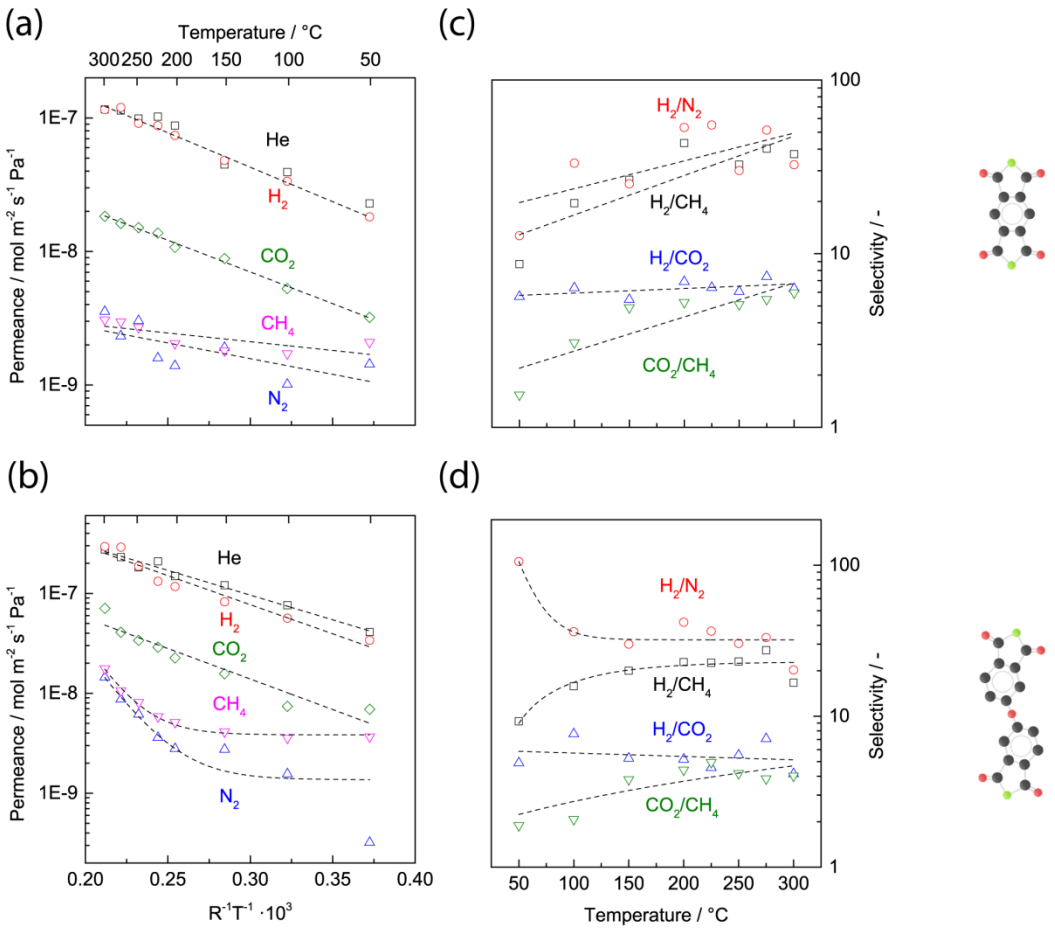

Figure S1. Arrhenius plot of the logarithm of the single gas permeance of He, H_2, CO_2, N_2 and CH_4, as a function of $R^{-1}\ T^{-1}\ \cdot 10^3$ for the polyPOSS-imides derived from PMDA (a), and ODPA (b). The activation energies are calculated from the slope of the ln(permeance) as function of 1 $R^{-1}T^{-1}$. The corresponding ideal gas selectivities of H_2/N_2, H_2/CH_4, H_2/CO_2 and CO_2/CH_4 as a function of temperature for the polyPOSS-imides derived from PMDA (c) and ODPA (d). The dashed lines are drawn as a guide to the eye.

Table S1 shows the apparent activation energies for permeance for all polyPOSS-imides prepared with PMDA, BPDA, ODPA and BPADA. The apparent activation energies for permeance are relatively high compared to conventional polymeric membranes. BPDA based polyPOSS-imides show particularly high activation energies, and underlines the high energy barriers for gas diffusion due to rigidity of the short imide bridge.

Table S1. The apparent activation energies for gas permeance for all polyPOSS-imides prepared with PMDA, BPDA, ODPA and BPADA. The activation for N_2 and CH_4 permeance of ODPA and BPADA based polyPOSS-imides were omitted due to changes in the apparent activation energy as function of temperature, in the temperature range of 50-300 °C.

	Activation energy / kJ mol^{-1}			
Gas	PMDA	BPDA	ODPA	BPADA
He	10.7	16.2	13.4	8.4
H_2	11.9	15.8	11.2	7.6
CO_2	10.9	15.26	14.1	4.4
N_2	5.4	13.17		
CH_4	3	7.78		

Thermogravimetric analysis. Thermogravimetric analysis (TGA) was performed on a STA 449 F3 Jupiter® (Netzch, Germany), equipped with a TG-only sample holder. Measurements were performed under 70 ml min^{-1} synthetic air (20% O_2 in N_2) or 70 ml min^{-1} nitrogen from room temperature to 1000 °C, with heating rates of 10 °C min^{-1}. Temperature calibration was performed using melting standards. Blank corrections with an empty cup were carried under the same heating program. Sample weights were determined ex-situ. Figure S2 shows the relative weight normalized for the initial weight as function of temperature, for the polyPOSS-imides thermalized under air and nitrogen atmosphere. All polyPOSS-imides in air and nitrogen atmosphere show a similar degradation offset temperature at a temperature above 300 °C. The initial mass loss at temperatures below 300 °C is likely due to evaporation of adsorbed water. The weight loss between 300-500 °C follows a similar degradation mechanism for all polyPOSS-imides. The weight loss rate under nitrogen atmosphere is significantly lower than under air atmosphere, suggesting that carbonaceous degradation products are only partially removed in the absence of oxygen. Above 500 °C, the weight loss rate decreases. Under air atmosphere the weight loss stabilizes for all imide bridge types,

except for BPADA based polyPOSS-imides. The distinct degradation process of the BPADA based polyPOSS-imide can be rationalized by the presence of the relatively stable quaternary carbon groups that are not present in the other polyPOSS-imides. Under nitrogen weight loss persists for all polyPOSS-imides, suggesting the degradation kinetics are relatively low in the absence of nitrogen.

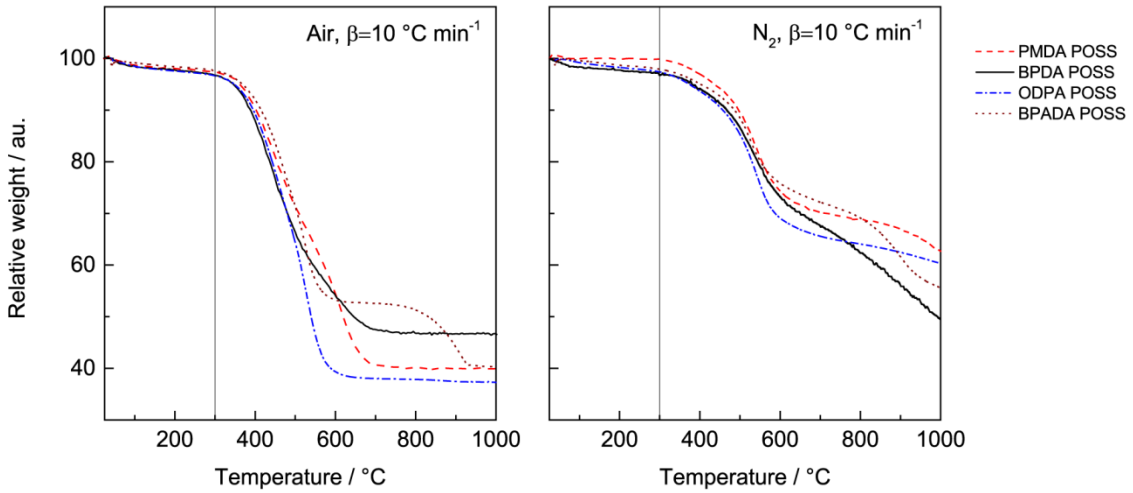

Figure S2. TGA mass loss curves of polyPOSS-imides prepared using PMDA, BPDA, ODPA and BPADA.

Differential scanning calorimetry. Differential scanning calorimetry (DSC) was performed on a DSC 8000 (Perkin Elmer, USA). Free standing polyPOSS-imide was placed in an aluminum sample pan and cycled from 50 to 300 °C with a heating rate of 20 °C min^{-1}. Measurements were performed under 70 ml min^{-1} nitrogen. Temperature calibration was performed using melting standards. Blank corrections with an empty cup were carried under the same heating program. Sample weights were determined ex-situ. Four subsequent heating and cooling cycles were used to eliminate the influence of adsorbed water on the measurement. Figure S3 shows the heat flow of all polyPOSS-imides as function of temperature, corrected for a blank run and sample weight. The heat flow curves of all polyPOSS-imides display no transitions,

underlining the lack of a glass transition in the material at temperatures up to 300 °C. The heat capacity, represented by the slope of the curves, is largest for the BPDA based polyPOSS-imide. The ODPA based polyPOSS-imide has the lowest calculated heat capacity. The PMDA and BPADA based polyPOSS-imides have similar heat flow profiles, suggesting the heat capacities are similar.

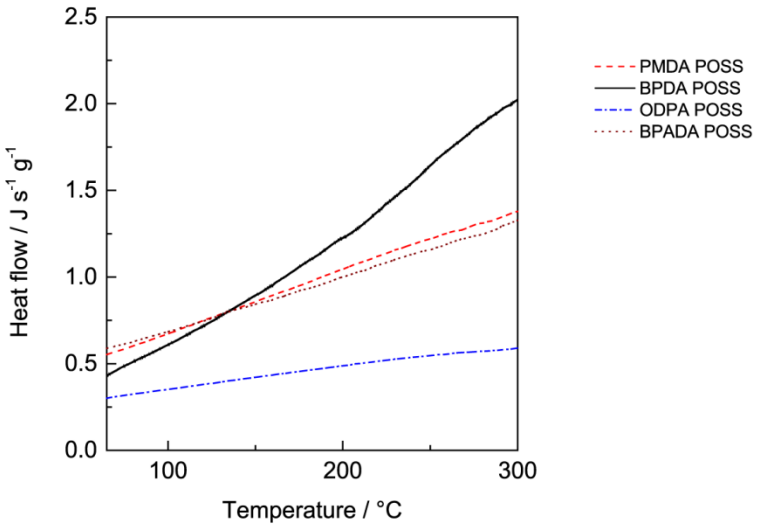

Figure S3. DSC curves of polyPOSS-imide prepared using PMDA, BPDA, ODPA and BPADA.

X-ray photoelectron spectroscopy. X-ray photoelectron spectroscopy measurements were performed on a Quantera SXM scanning XPS microprobe (Physical Electronics), using a monochromatic Al Kα source (1486.6 eV). Octa-ammonium POSS powder and polyPOSS-imide on α-alumina discs coated with 3 μm thick γ-alumina samples were measured. The elemental compositions of the polyPOSS-imides and octa-ammonium POSS powder are given in Table S2. For all polyPOSS-imide samples an increase in carbon and oxygen content with respect to the POSS is observed, originating from imide bridge formation. The remaining sodium and chlorine are originating from the aqueous alkaline POSS solution.

Table S2 Elemental compositions of the polyPOSS-imides and octa-ammonium POSS powder.

	Element					
Sample	C1s	N1s	O1s	Na1s	Cl2p	Si2p
Octa-ammonium POSS	47.8	9.8	22.0	0.8	9.0	11.5
PMDA based polyPOSS-imide	39.7	4.3	39.7	3.2	0.08	11.3
BPDA based polyPOSS-imide	42.7	4.8	37.8	2.5	0.1	10.3
OPDA based polyPOSS-imide	55.4	5.2	29.2	1.1	0.11	7.8
ODPDA based polyPOSS-imide	61.2	4.3	26.3	0.3	0.03	7.7

The average number of imide bridged per POSS cage is calculated from the Si/C, Si/N and Si/O ratios of the polyPOSS-imides. For all polyPOSS-imides around 4 out of 8 functional groups on each POSS cage are bridged with an imide moiety. The absence of anhydride and carboxylic acid peaks in the FTIR-ATR spectra suggests that the imide bridges are connected with two POSS moieties. The carbon (C1s) and nitrogen (N1s) elemental spectra of octa-ammonium POSS powder and polyPOSS-imides are shown in Figure S4. The main differences between the C1s elemental spectrum of the polyPOSS-imides and the octa-ammonium POSS originates from the imide bonds and additional aliphatic and aromatic carbon groups. The emerged binding energy peak of the imide groups at 288 eV is most pronounced. The deconvoluted peak surface area corresponds to a number of 4 imide groups per POSS cage. This in agreement with the nitrogen spectral data. The nitrogen elemental fit of octa-ammonium POSS shows two distinct peaks, attributed to the ammonia (401 eV) and amine (398.7) binding energies of the partially deprotonated ammonia groups. All polyPOSSimide nitrogen spectra show a distinct shift towards lower binding energy groups. The shift can be attributed to an increase in amine and imide bond contribution to the N1s spectrum. About 50% of the nitrogen bonds in the deconvoluted N1s spectra can be attributed to imide groups. Table S3 gives the deconvoluted peak area distribution for the different binding energies associated with imide, amine and ammonia groups. The data suggests that around 4 out of 8 functional groups on each POSS cage are bridged with an imide moiety.

This is in good agreement with the calculated numbers from the elemental ratios and with previously found results for 6FDA based polyPOSS-imides.

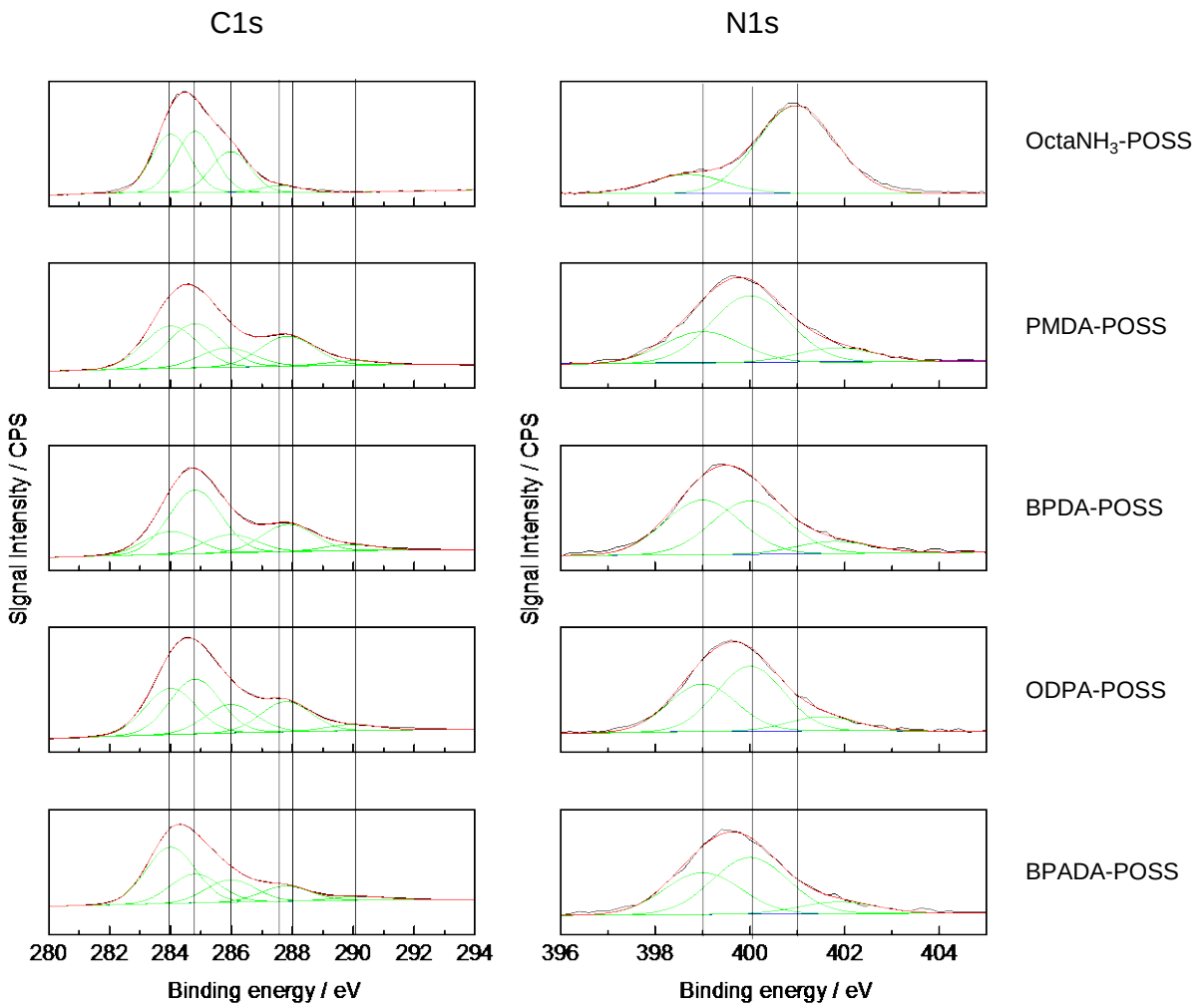

Figure S4. Deconvoluted XPS elemental spectra of C1s and N1s for polyPOSS-imides prepared using PMDA, BPDA, ODPA and BPADA.

Table S3. Deconvoluted XPS peak area distribution for the binding energies associated with amine, imide and ammonia binding energies

	Deconvoluted peak area		
	imide (%)	amine (%)	ammonia (%)
PMDA	51.1	38.0	10.9
BPDA	59.5	27.8	12.7
OPDA	51.2	37.6	11.2

ODPDA	44.5	45.6	9.9
Octa-NH3-POSS	0	17.7	82.3

Figure S5 shows the deconvoluted XPS elemental spectra of Si2p and O1s for octa-ammonium POSS and the polyPOSS-imides prepared with the different dianhydrides. The single binding energy of the Si2p spectrum of the octa-ammonium POSS corresponds to the attributed to the SiO_3C groups of the POSS cage.

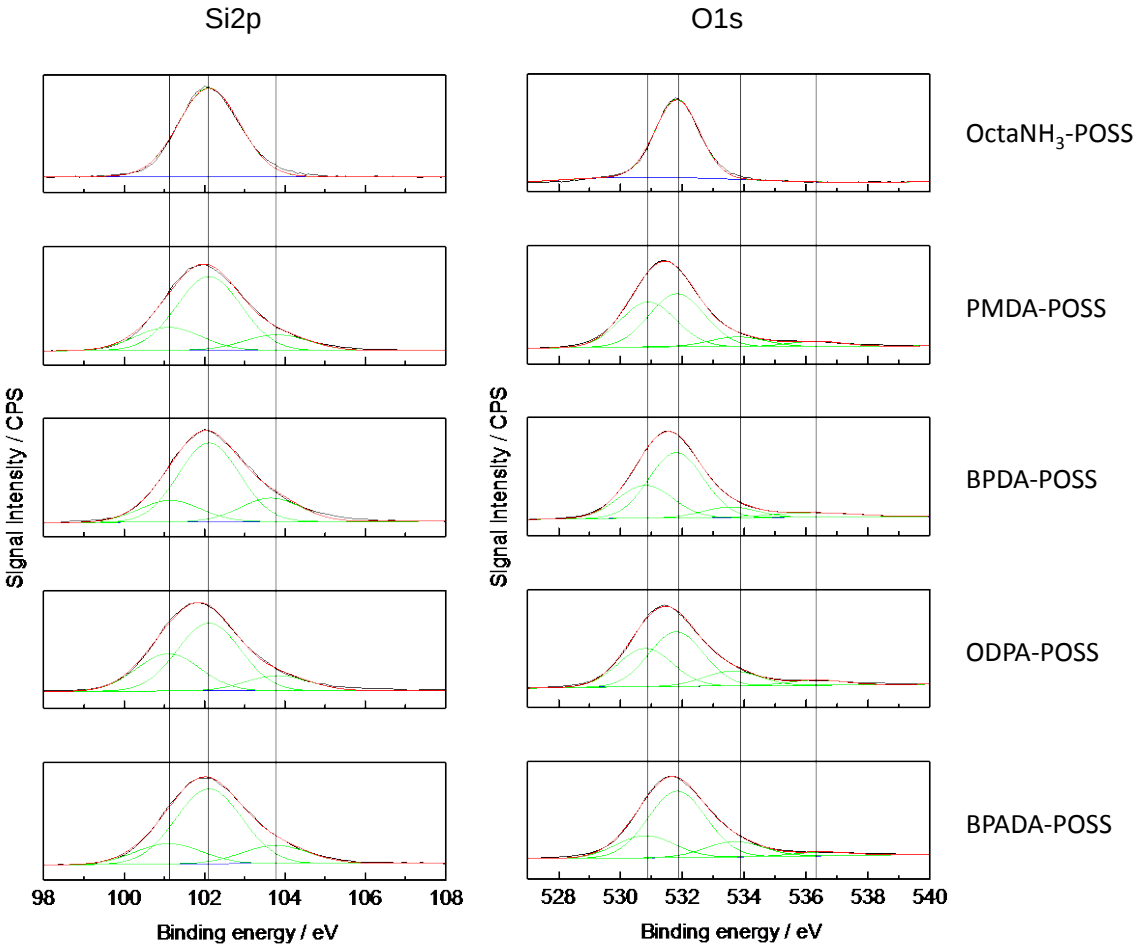

Figure S5. Deconvoluted XPS elemental spectra of Si2p and O1s for polyPOSS-imides prepared using PMDA, BPDA, ODPA and BPADA.

The polyPOSS-imide Si2p spectra display a shift in binding energies towards both lower and higher binding energies. These peaks are associated with silanol and SiO- formed by partial hydrolysis of the POSS cage. The shift in binding energy and broadening of the XPS

spectrum is mainly attributed to the formation of silanol groups. The single binding energy of the O1s spectrum of the octa-ammonium POSS corresponds to the siloxane bonds in the POSS cages. The O1s spectrum of the polyPOSS-imides show additional peaks at a binding energy of 530.7 and 532.6 eV, associated with the C=O of the imide group and silanol bonds, respectively. The appearance of the silanol peak in the O1s spectrum is in agreement with the Si2p spectrum of the polyPOSS-imide samples.

Attenuated Total Reflection – Fourier Transform Infrared Spectroscopy. The chemical structures of the polyPOSS-(amic acid) and polyPOSS-imide were analyzed with Attenuated Total Reflection Fourier Transform Infrared Spectroscopy (ATR-FTIR) of free standing films using an ALPHA FT-IR Spectrometer (Bruker Optics Inc, Germany) equipped with a ZnSe crystal. All spectra were recorded at room temperature. Figure S6 shows the FTIR-ATR absorbance spectra of polyPOSS-imides prepared with PMDA, BPDA, ODPA and BPDADA. The octa-ammonium POSS and PMDA spectra are given as reference. The dianhydride peaks at 1820 and 1870 cm^{-1} for PMDA are not reflected in any of the polyPOSS-imide spectra. The ammonia and water related peaks at 3200-2800 cm^{-1} are clearly visible in the octa-ammonium POSS spectrum. The polyPOSS-imides absorbance spectra only show slight absorbance in this region, underlining the absence of any carboxylic acid and ammonia groups in the polyPOSS-imide layers. Table S4 and S5 show the bond and vibrational mode data as function of peak position for the polyPOSS-(amic acid) and polyPOSS-imides respectively.

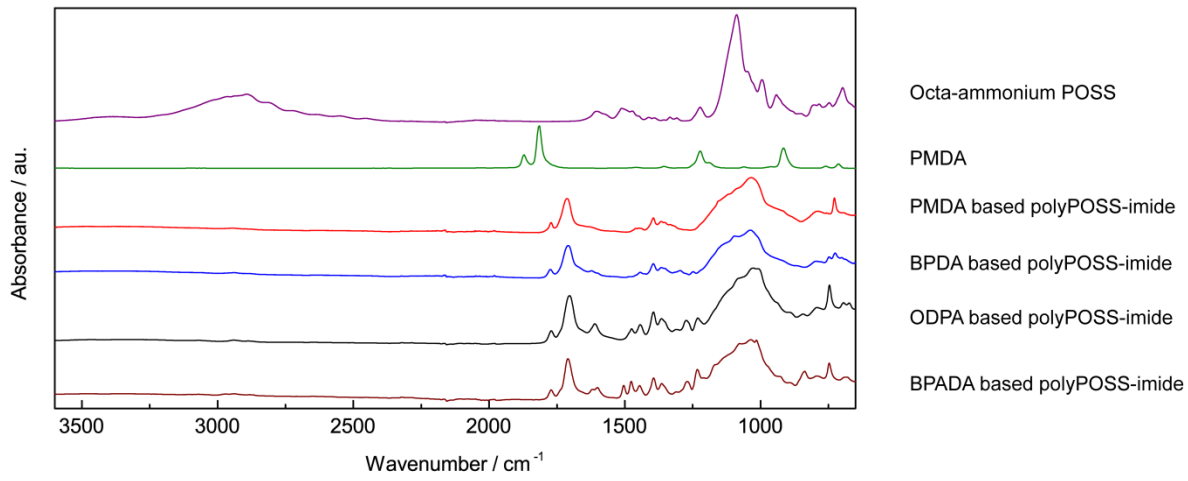

Figure S6 FTIR-ATR absorbance spectra of polyPOSS-imides prepared with PMDA, BPDA, ODPA and BPDADA. The octa-ammonium POSS and PMDA spectra are given as reference. The PMDA spectrum is adapted from the NIST chemistry webbook.[1]

Table S4 PolyPOSS-(amic acid) bond and vibrational mode data as function of peak wavenumber position, for the polyPOSS-imides prepared with PMDA, BPDA, ODPA and BPDADA.

PolyPOSS-(amic acid)						
	PMDA	BPDA	ODPA	BPADA		
Wavenumber	Intensity	Intensity	Intensity	Intensity	Bond	Vibrational mode
cm^{-1}						
693	medium	medium	medium	medium	C-H	out of plane bend
727	shoulder	shoulder	shoulder	shoulder		O-substituted benzene
746	-	low	medium	medium	CH	out of plane bend 1,2,4, trisubstituted benzene
773	shoulder	shoulder	shoulder	shoulder	NH	def vib amide
798	medium	medium	medium	medium	NH_2	out of plane bend of primary amine
837	-	-	low	medium	NH_2	out of plane bend of primary amine
910	shoulder	shoulder	shoulder	shoulder	C-C	rocking
955	shoulder	shoulder	shoulder	shoulder	C-C	rocking
1000	shoulder	shoulder	shoulder	shoulder	C-C	rocking
1040	high	high	high	high	Si-O cage	str
1093	high	high	high	high	Si-O ladder	str
1120	shoulder	shoulder	shoulder	shoulder	C-H	in plane bending
1203	medium	medium	medium	medium	N-H	def
1228	-	-	medium	high	C-O (ether)	str

1272	-	-	medium	medium	C-O-C (ether)	def vib
1370	low	low	medium	high	C=O or C-N	str
1400	medium	medium	high	high	C=O or C-N	str
1445	low	low	medium	medium	CH_2	scissoring
1475	-	-	medium	medium	CH_2	def vib
1504	-	-	-	medium	C=C	srt (only for electron donor groups)
1560	high	high	high	high	N-H	bend amide
1620	high	high	high	high	C=O	str amide
1670	high	high	high	high	C=O	str carboxylic acid
1710	-	-	-	-	C=O	asym str imide
1770	-	-	low	-	C-O-C	sym str
1845	-	-	low	-	C-O-C	asym str
2878	medium	medium	medium	medium	CH_2	sym str
2939	medium	medium	medium	medium	CH_2	asym str
3068	low	low	low	low	H_2O/COOH	bend
3235	broad	broad	broad	broad	H_2O/COOH	OH str
3380	broad	broad	broad	broad	NH_2	asym str

Table S5 PolyPOSS-imide bond and vibrational mode data as function of peak wavenumber position, for the polyPOSS-imides prepared with PMDA, BPDA, ODPA and BPDADA.

PolyPOSS-imide						
	PMDA	BPDA	ODPA	BPADA		
Wavenumber	Intensity	Intensity	Intensity	Intensity	Bond	Vibrational mode
cm^{-1}						
693	medium	medium	medium	medium	C-H	out of plane bend
725	medium	medium	low	low	N-H	wagging
746	-	low	medium	medium	CH	out of plane 1,2,4, trisubstituted benzene
773	shoulder	shoulder	shoulder	shoulder	NH	def vib amide
793	low	low	low	low	NH_2	out of plane bend of primary amine
837	-	-	low	medium	NH_2	out of plane bend of primary amine
910	shoulder	shoulder	shoulder	shoulder	C-C	rocking
965	shoulder	shoulder	shoulder	shoulder	C-C	rocking
1000	shoulder	shoulder	shoulder	shoulder	C-C	rocking
1040	high	high	high	high	Si-O cage	str
1093	high	high	high	high	Si-O ladder	str
1120	shoulder	shoulder	shoulder	shoulder	C-H	in plane bending
1228	-	-	high	high	C-O (ether)	str
1272	-	-	medium	medium	C-O-C	def vib
1364	low	low	medium	medium	C=O or C-N	str
1393	medium	medium	high	high	C=O or C-N	str
1445	low	low	medium	medium	CH_2	scissoring
1475	-	-	medium	medium	CH_2	def vib

1504	-	-	-	medium	C=C	srt (only for electron donor groups)
1610	-	-	medium	medium	C=O	str amide
1670	-	-	-	-	C=O	str carboxylic acid
1710	high	high	high	high	C=O	asym str imide
1770	low	low	low	low	C=O	sym str imide
2878	medium	medium	medium	medium	CH_2	sym str
2939	medium	medium	medium	medium	CH_2	asym str
3068	low	low	low	low	H_2O/COOH	bend
3235	broad	broad	broad	broad	H_2O/COOH	OH str
3380	broad	broad	broad	broad	NH_2	asym str

1. Stein, S. E., *Infrared Spectra*. NIST Mass Spec Data Center.